

International Journal of Mechatronics and Manufacturing Systems

ISSN online: 1753-1047 - ISSN print: 1753-1039

<https://www.inderscience.com/ijmms>

Effect of material inhomogeneity on chatter stability

Nevzat Bircan Bugdayci, Martin Postel, Konrad Wegener

DOI: [10.1504/IJMMS.2022.10051493](https://doi.org/10.1504/IJMMS.2022.10051493)

Article History:

| | |
|-------------------|------------------|
| Received: | 14 March 2022 |
| Accepted: | 23 June 2022 |
| Published online: | 28 November 2022 |

Effect of material inhomogeneity on chatter stability

Nevzat Bircan Bugdayci*, Martin Postel
and Konrad Wegener

Institute of Machine Tools and Manufacturing (IWF),
ETH Zürich,

Zürich, Leonhardstrasse 21, CH-8092, Switzerland

Email: bugdayci@iwf.mavt.ethz.ch

Email: postel@iwf.mavt.ethz.ch

Email: wegener@iwf.mavt.ethz.ch

*Corresponding author

Abstract: Chatter vibrations in milling are a widely researched topic in manufacturing science. The models used to predict and mitigate chatter use assumptions for the model inputs. Assuming the workpiece material is homogenous, is such an assumption. In this study, the effect of workpiece material variation on chatter stability is studied. Upon the observation of varying stability limits during milling operations of aluminium blocks, it is shown that the workpiece material inhomogeneity affects the chatter stability. To support this hypothesis, the surface hardness of the workpieces is measured using the Leeb rebound hardness test method. It is shown that the location-dependent chatter stability limits, calculated using the local cutting coefficients, capture the position-dependent stability nature of the experimental data.

Keywords: chatter stability; milling; hardness; material inhomogeneity; stability lobe diagrams; chatter vibrations; stability limits; Vickers hardness; cutting coefficients.

Reference to this paper should be made as follows: Bugdayci, N.B., Postel, M. and Wegener, K. (2022) 'Effect of material inhomogeneity on chatter stability', *Int. J. Mechatronics and Manufacturing Systems*, Vol. 15, No. 4, pp.264–285.

Biographical notes: Nevzat Bircan Bugdayci received his PhD in 2022 from ETH Zürich, Switzerland. He received his BSc (2011) from METU, Ankara, Turkey and his MSc (2013) from Koc University, Istanbul, Turkey in Mechanical Engineering. His research interests include process modelling, process monitoring and machine learning in the field of machining.

Martin Postel received his PhD in 2020 from ETH Zürich, Switzerland. He received his BSc (2012) and MSc (2015) in Mechanical Engineering from the Technical University of Darmstadt, Germany, with research stays at Ecole Centrale Lyon, France, and at the University of British Columbia, Canada. His research interests include chatter stability, machine tool dynamics and machine learning in the field of metal cutting operations.

Konrad Wegener received his PhD in 1990 from the TU Braunschweig, Germany. He has been a Full Professor and the Head of the Institute of Machine Tools and Manufacturing at ETH Zurich since October 2003 and leads the manufacturing section of the Swiss transfer centre Inspire AG.

His fields of research interests are optimisation of machine tools, cutting technology, additive manufacturing, laser material processing and electrical discharge machining.

1 Introduction

The manufacturing research community has been trying to find methods and approaches that yield accurate and practical solutions to the frequently encountered chatter problem for many years. One of the most important challenges in chatter vibration simulations is the accurate and precise determination of the cutting force coefficients as stated by leading researchers in the field like Arrazola et al. (2013) and Altintas et al. (2014). There are many studies in the literature that aim to improve the accuracy of these coefficients' identification. Budak et al. (1996) proposed an approach, where these cutting coefficients are calculated using a set of standard orthogonal data, instead of mechanistic calibration tests. Berezvai et al. (2018) investigated the variation of the shear angle during orthogonal cutting processes experimentally for stationary and non-stationary cutting, based on high-speed camera recordings and cutting force measurements. Layegh and Lazoglu (2014) presented a new and accurate strategy for estimation of cutting coefficients for ball-end milling of free form surfaces, by dividing the ball region in thin disks and finding the contribution of each disk by designing an experimental setup in which only that disk is engaged with the workpiece. Denkena et al. (2014) presented a force model for the identification of the cutting force coefficients which do not require these special calibration experiments. Denkena et al. (2014) also presented a tool wear monitoring system based on monitoring of these cutting force coefficients. Stepan et al. (2011) studied the connection between the sensitivity of the dynamics of regenerative cutting and the non-linearity of these cutting coefficients. Aggarwal et al. (2013) tried to obtain the tangential component of these cutting coefficients from the cutting torque, calculated from the spindle motor current. Altintas (1992) used the current drawn by feed drive motors for cutting force monitoring and showed that tool failure in milling can be detected using this approach. Campocasso et al. (2017) obtained the cutting coefficients by inverse identification from turning tests and showed that cutting forces can be estimated using shear tests. Besides the identification of these coefficients, the variation of these coefficients with respect to various process parameters were also investigated in literature. For example, Grossi et al. (2014) investigated the variation of the cutting coefficients with respect to the cutting speed in milling Aluminium 6082-T4 alloy and showed the dependence of the cutting coefficients on the cutting speed especially for high speed milling. Recently Pérez-Ruiz et al. (2021) examined the effects of laser powder bed fusion process parameters on cutting forces and the anisotropy of alloys in milling of Inconel 718 in which they proposed a Taylor based model to quantify the crystallographic effects on the shear strength. Their analysis revealed a significant interaction between the direction of the plane of the shear band and the grain orientation along the main axis. Urbikain and Olvera (2020) used a feed linearisation approach in which the cutting coefficients are obtained by interpolation from different spindle speeds and depth of cuts to model cutting forces and resulting surface topography for serrated end mills. Gomez et al. (2020) suggested a new approach for force and stability prediction for inserted end and face mills using a reverse engineering approach, where

they used structured light scanning to identify the spatial coordinates of the points that define the multiple insert cutting edges. Later, No et al. (2020) analysed these points to extract the cutting edge radius and angle values, which are then incorporated in a time domain simulation that predicts cutting force and tool/workpiece deflection for user-selected operating parameters to achieve good agreement between predicted and measured cutting forces.

Despite these numerous studies, the complexity of the problem still makes it difficult to maximise both practicality and accuracy of these models simultaneously. Consequently, accuracy is sometimes overlooked in favour of convenience in practice. Assuming homogeneous material characteristics for the whole workpiece is such a convenience. In the presented literature, the cutting coefficients are modelled or calibrated for a tool-material combination, and the same coefficients are used to calculate the stability lobes for the whole workpiece geometry as explained by Altintas (2012). While the constant cutting coefficient assumption used in these studies, is convenient for most modelling efforts, in reality, a slight variance in cutting coefficients can cause a sudden ‘qualitative’ change in the system’s behaviour around the stability border as investigated by Honeycutt and Schmitz (2019). The constant cutting coefficient approach is therefore insufficient to explain the stability variation during stationary cuts with constant cutting parameters and tooltip dynamics. In this study, it is shown that the local material hardness affects the local stability behaviour. It is also shown that the accuracy of the stability predictions increases when the local hardness variation is taken into account in the stability prediction models. Using the approach presented in this study, the cutting coefficients for a batch of inhomogenous workpieces can be calibrated using a low cost rebound hardness measurement test, once a single prototype workpiece is used for calibration with a dynamometer.

2 Motivation

During the milling operations performed using a particular batch of EN AW-6082 Aluminium alloy blocks that were cut out of rolled thick plates, it was observed that the dynamic stability was changing along the cut, as shown in Figure 1. The hardness values were measured along the feed direction as indicated with the red arrow. The tool was a 12 mm helical end mill with two cutting flutes. The spindle speed was 9100 rpm, the feed rate was 0.02 mm/tooth, which corresponded to 364 mm/min, and the depth of cut was 1.1 mm. The cuts were slot milling operations. The sound spectrum of the cut is also given in Figure 1, which shows that the chatter stability followed a similar trend as the measured hardness values, i.e., chatter occurred at the beginning of cut where hardness values were relatively higher, then stopped when the hardness dropped and towards the end of the cut reoccurred with increasing hardness.

Here it must be noted that the hardness measurements are conducted using a rebound hardness testing method which will be explained in Section 3 – Material Characterisation. The point-wise nature of the measurements is a contributing factor to the discrepancy between the measured hardness levels and the observed stability.

Since the process parameters were constant throughout the cut, first, the tooltip FRFs were checked at various locations along the cut, as shown in Figure 2 to investigate whether they could explain the varying stability. The workpiece, which was a cube with 120 mm edge length, was divided into a $5 \times 5 \times 5$ grid as shown in Figure 2. In order to

observe the effect of feeding along the X -axis on the tooltip FRFs, the tool-tool holder assembly was moved along the X -axis with increments of 24 mm at a constant Y position of $Y = 60$ mm, which corresponded to the symmetry axis of the workpiece. At each measurement location, which is indicated with a yellow cross in Figure 2, FRFs were measured.

Figure 1 Effect of material inhomogeneity on chatter stability (see online version for colours)

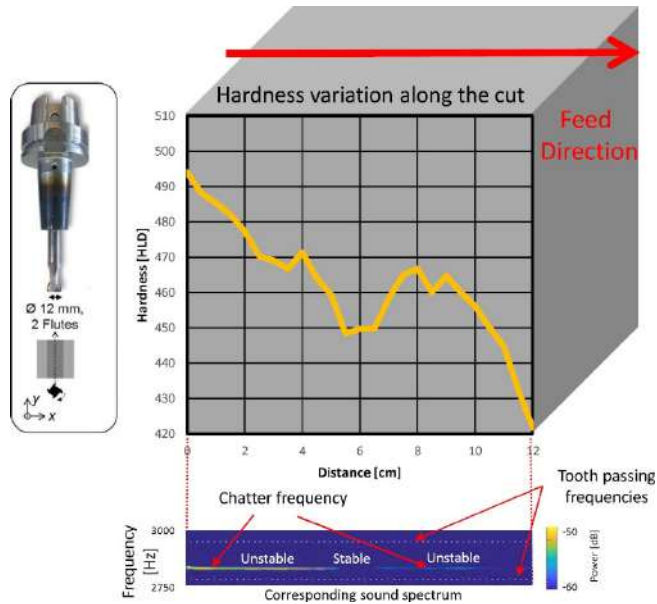
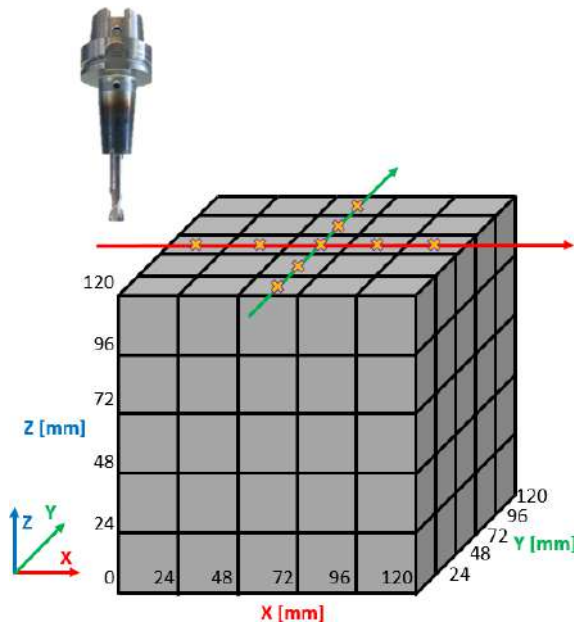
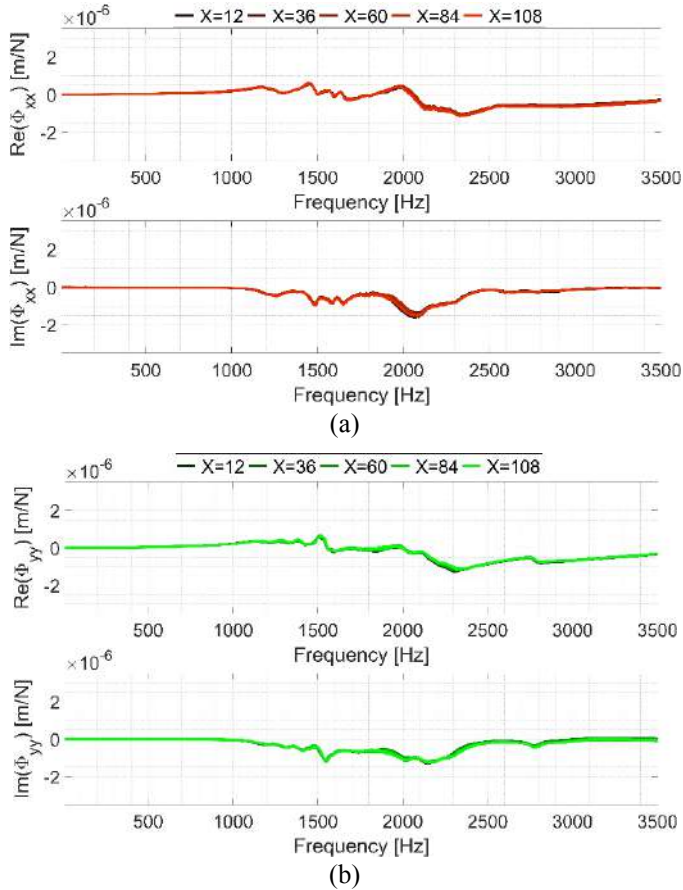


Figure 2 Locations of the tooltip FRF measurements (see online version for colours)



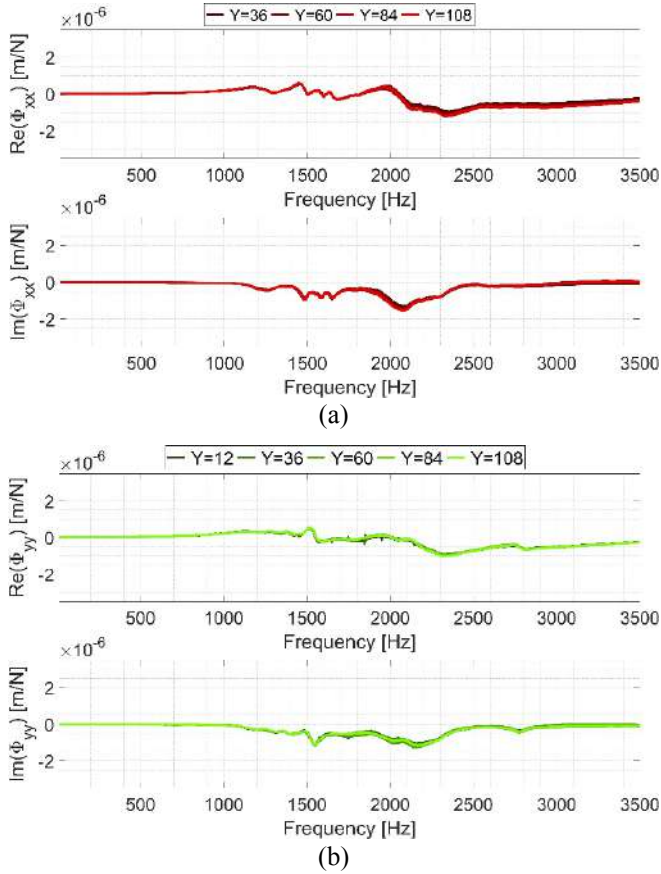
The measurements were conducted on the tool tip by fixing a 1D Bruel & Kjaer accelerometer on the tool tip and impacting the tool using a Kistler type 9722 impulse hammer. Figure 3(a) shows the FRF measurements in the X direction and Figure 3(b) shows the FRF measurements in the Y direction.

Figure 3 (a) TCP FRF measurements in the X direction for different X positions and constant Y position ($Y = 60$ mm) as shown in Figure 2 and (b) TCP FRF measurements in the Y direction for different X positions and constant Y position ($Y = 60$ mm) as shown in Figure 2 (see online version for colours)



Similarly, in order to observe the effect of feeding along the Y -axis on the tooltip FRFs, the same approach was repeated in the Y direction. The tool-tool holder assembly was moved along the Y -axis with increments of 24 mm at a constant position $X = 60$ mm. FRFs were measured at locations indicated in Figure 2. Figure 4(a) shows the FRF measurements in the X direction and Figure 4(b) shows the FRF measurements in the Y direction.

Figure 4 (a) TCP FRF measurements in the X direction for different Y positions and constant X position ($X = 60$ mm) as shown in Figure 2 and (b) TCP FRF measurements in the Y direction for different Y positions and constant X position ($X = 60$ mm) as shown in Figure 2 (see online version for colours)



From Figure 3(a) and (b), it is seen that along the X -axis, the TCP FRFs were unaffected by the position. Similarly, Figure 4(a) and (b) show that the tooltip dynamics were almost constant along the Y -axis. Next, the workpiece responses were measured to rule out any effect that might be coming from the changing workpiece dynamics along the cut. For this purpose, the 1D Bruel & Kjaer accelerometer also used for the tool tip FRF measurements are fixed on the locations indicated with the magenta cross on Figure 5 and the workpiece is excited using the Kistler type 9722 impulse hammer on the other side of the workpiece.

Figure 6(a) and (b) show the workpiece dynamics along the cut. It is important to note the difference in scales while comparing Figure 6 with Figures 3 and 4 since the workpiece responses are two orders of magnitude smaller than the TCP FRFs. While there is a slight difference in workpiece response FRFs as seen in Figure 6(a) and (b), this difference is not sufficient to explain the stability variation because of two reasons. First, the difference is negligible compared to the tooltip FRFs. Second, the workpiece FRFs are monotonically changing while the stability state changed from unstable to stable and back to unstable.

Figure 5 Locations of the workpiece FRF measurements (see online version for colours)

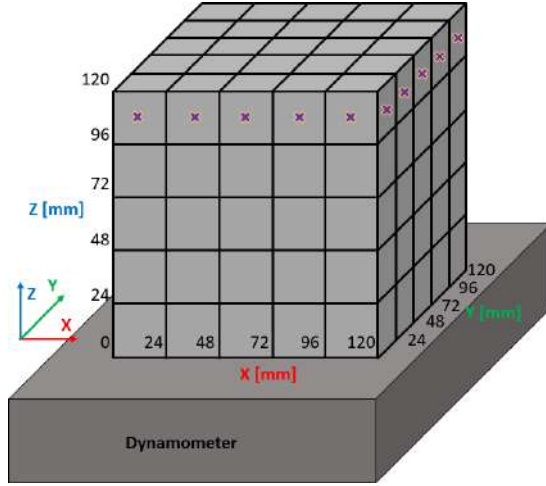


Figure 6 (a) Workpiece FRF measurements in the Y direction along the X-axis at points indicated in Figure 5 and (b) Workpiece FRF measurements in the X direction along the Y-axis at points indicated in Figure 5 (see online version for colours)

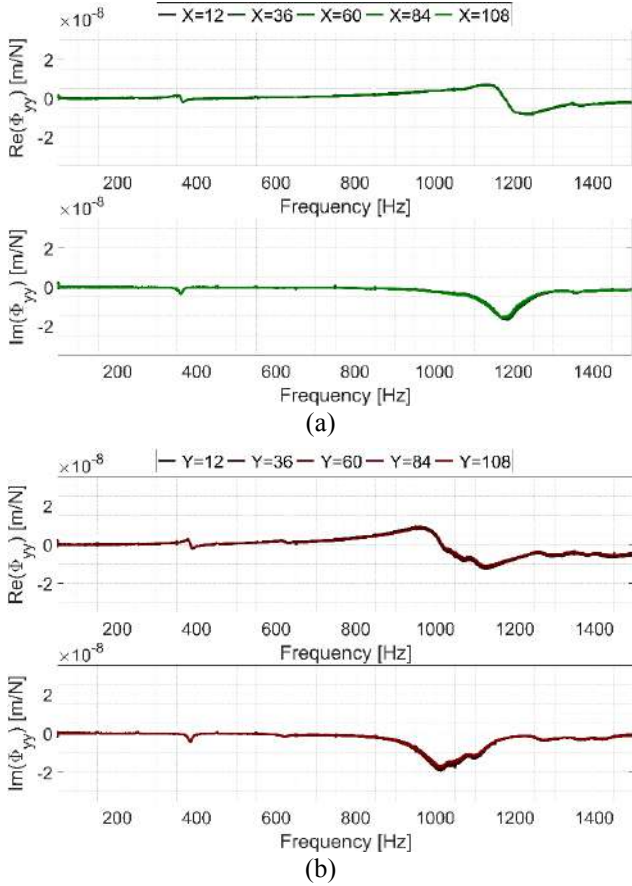
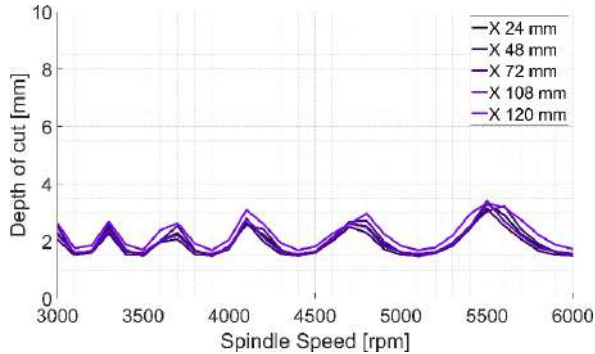


Figure 7 shows the effect of the varying combined dynamics along the X -direction on the resulting stability limits. Even though the variation in the tooltip dynamics affects the stability slightly (increasing the stability limit around 5%), it does not explain the re-occurrence of the chatter towards the end of the cut.

Figure 7 Corresponding SLDs for varying tool tip FRFs at different positions in X -direction and $Y = 60$ mm are shown in Figure 2 (see online version for colours)



The fact that the TCP FRFs remained constant while the chatter vibrations restarted after having been suppressed along the cut indicates that the changing stability was not related to changing frequency response but to the excitation force. Since the cutting parameters such as the spindle speed, feed rate, depth of cut, and width of cut were constant along with the cuts in Figure 1, it is concluded that the variation is due to the inhomogeneity of the workpiece material resulting from the primary manufacturing process, in this case – rolling, as investigated by Mrowka et al. (2009).

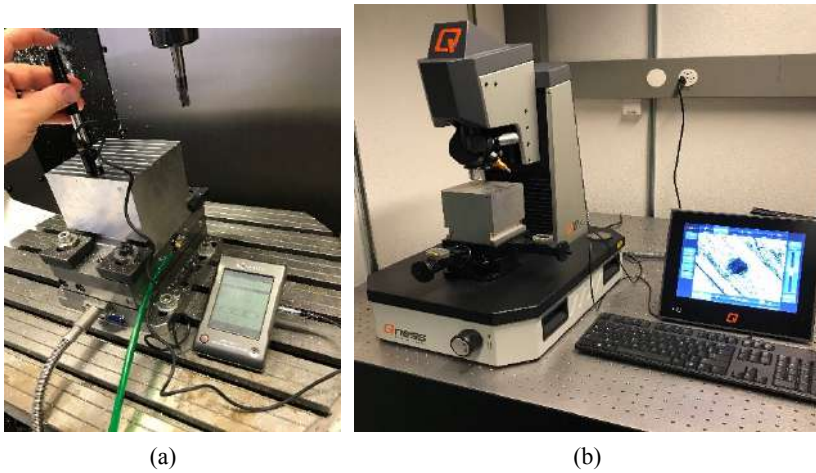
3 Material characterisation

In order to identify the inhomogeneity of the workpiece materials, Leeb rebound hardness testing method is utilised. In Leeb hardness testing method, a spring-powered hardball hammer tip is used for impact. The velocity of the hammer is measured electronically while it moves towards (v_i) and away (v_r) from the target. The Leeb hardness value is defined as:

$$HLD = 1000 \cdot \frac{v_r}{v_i} \quad 1)$$

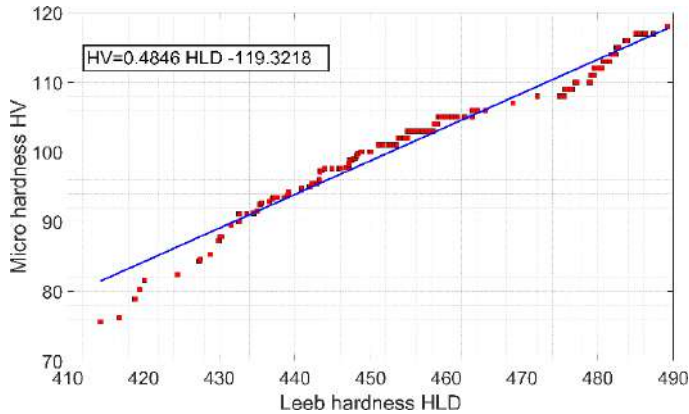
The result is Leeb hardness from 0 to 1000 which can be calibrated to other hardness scales such as Rockwell and Vickers. According to ISO 16859 (2016) standards, the Leeb rebound hardness testing can be used in the range of 300 HLD–890 HLD. It should be noted that, in this study, it is assumed that the surface hardness measurements represent the relative local hardness and the hardness variation along the cut is not considered. For the rebound hardness measurements in this work, a Sauter HMO mobile Leeb hardness tester was used, as shown in Figure 8(a).

Figure 8 (a) Sample measurement of the surface hardness using Sauter HMO Leeb hardness measurement and (b) Qness micro hardness tester (see online version for colours)



The aluminium blocks used in this study were $120 \times 120 \times 120$ mm (W \times H \times L) in size. A five-by-five grid with 24 mm edge length was drawn at each surface of the block, as shown in Figures 2 and 5. Five hardness measurements were conducted for each square element on the grid to have statistically significant results. The workpiece hardnesses of the blocks were also measured using Qness micro hardness device shown in Figure 8(b), which utilises the Vickers microhardness test method for comparison. By fitting a linear regression model, the Leeb hardness measurements were compared with respect to the Vickers microhardness measurements for Al-6082. Figure 9 presents the correlation between microhardness and rebound hardness measurements.

Figure 9 Comparison of the rebound hardness (see online version for colours)



4 Derivation of the hardness dependent local cutting coefficients

Once it was determined that the workpieces were not homogeneous, the position-dependent local material properties were used to predict position-dependent local cutting

coefficients. First, the local hardness of the material is written as a function of the location as follows:

$$HV = HV(x, y, z). \quad (2)$$

Next, the local hardness values were used to calculate the local shear stress. Costa et al. (2015) studied the relation between the material hardness and local tensile properties of Al-6082. They showed that there is a linear relation between the yield stress and the Vickers hardness. Thus, the local yield stress can be written as a function of local hardness:

$$R_{p,0.2}(x, y, z) = c_1 HV(x, y, z) + c_2 \quad (3)$$

Similarly, the local shear yield stress can be written as:

$$\tau_s(x, y, z) = c_3 HV(x, y, z) + c_4, \quad (4)$$

assuming the shear yield stress of a material is linearly correlated to the yield stress of that material as suggested by Budynas et al. (2011), with constants c_3 and c_4 being unknown. Once the assumption of a linear correlation between the local hardness and the local shear yield stress profile is made, fundamental cutting theory can be exploited to write the local cutting coefficients as a function of local material hardness. The cutting coefficients that relate the measured cutting forces to the tool geometry and material dependent terms are written by Altintas (2012) as follows:

$$K_{tc} = \tau_s \frac{\cos(\rho - \gamma)}{\sin \varphi_c \cos(\varphi_c + \rho - \gamma)}, \quad (5)$$

$$K_{fc} = \tau_s \frac{\sin(\rho - \gamma)}{\sin \varphi_c \cos(\varphi_c + \rho - \gamma)}, \quad (6)$$

where K_{tc} is the cutting force coefficient and K_{fc} is the feed force coefficient. Substituting equation (4) into equations (5) and (6), one can write the local cutting coefficients as a function of material properties and the tool geometry:

$$K_{tc}(x, y, z) = \tau_s(x, y, z) \frac{\cos(\rho - \gamma)}{\sin \varphi_c \cos(\varphi_c + \rho - \gamma)}, \quad (7)$$

$$K_{fc}(x, y, z) = \tau_s(x, y, z) \frac{\sin(\rho - \gamma)}{\sin \varphi_c \cos(\varphi_c + \rho - \gamma)}, \quad (8)$$

In this study, the workpiece material inhomogeneity was incorporated into the cutting coefficients by assuming that the shear stress in equations (7) and (8) is linearly correlated with the local hardness of the workpiece. While the friction angle and the shear angle are also dependent on the material properties, their effect on cutting coefficients was neglected in this study. Subsequently, a linear correlation between the local hardness measurements and the cutting coefficients is proposed as follows:

$$K_{tc}(x, y, z) = \frac{HV(x, y, z)}{HV} \overline{K_{tc}}, \quad (9)$$

$$K_{fc}(x, y, z) = \frac{HV(x, y, z)}{\overline{HV}} \overline{K_{fc}}, \quad (10)$$

where the lines above the parameters indicate average values. Following equations (9) and (10), the SLDs can be modified using the local hardness-dependent cutting coefficients to forecast the chatter stability with respect to the local workpiece material hardness. Tests showed that the variation of hardness along the width and depth of a slot milling cut is negligible compared to the variation of hardness along with the cut and the local cutting coefficients can be calculated by updating the average cutting force coefficients with the local hardness measurements along the cut.

5 Experimental results

To validate the aforementioned method, slot milling tests were done using a 12 mm Voha 022456120 end mill with four flutes, mounted on a Zürn HSK-A63 63.11.20.2 collet chuck. To identify the average cutting coefficients, the mechanistic calibration method described by Altintas (2012) was used. The parameters of the calibration tests are given in Table 1.

Table 1 Mechanistic calibration test conditions

| <i>Parameter</i> | <i>Value</i> |
|-----------------------|----------------------------------|
| Spindle speed | 4000–6000–8000–10000–12000 rpm |
| Feed rate | 0.01–0.02–...–0.14–0.15 mm/tooth |
| a_p | 1 mm |
| a_e | 12 mm |
| Number of flutes | 4 |
| Stick-out length | 55 mm |
| Number of repetitions | 3 |
| Feed direction | X+, Y+ |

In order to observe the effect of hardness on the cutting coefficients over the whole range of hardness variation, the calibration tests were conducted on surfaces with the highest, lowest, and median average hardness values. Figure 10 presents the mean and standard deviation of the hardness measurements of all 72 measured surfaces (on each of the six surfaces of 12 cubic workpieces). Table 2 gives the corresponding statistical values and Figure 11 shows the hardness variation on these surfaces in 2D colourmaps.

Table 2 Statistical hardness properties of the selected surfaces

| | μ | σ | <i>Corresponding workpiece</i> |
|---------|-------|----------|--------------------------------|
| Maximum | 485 | 2.4 | Workpiece L |
| Median | 469 | 5.9 | Workpiece E |
| Minimum | 405 | 10.4 | Workpiece I |

Figure 10 Mean (μ) and standard deviation (σ) of the hardness measurements for each surface of the 12 workpieces (In red, selected surfaces) (see online version for colours)

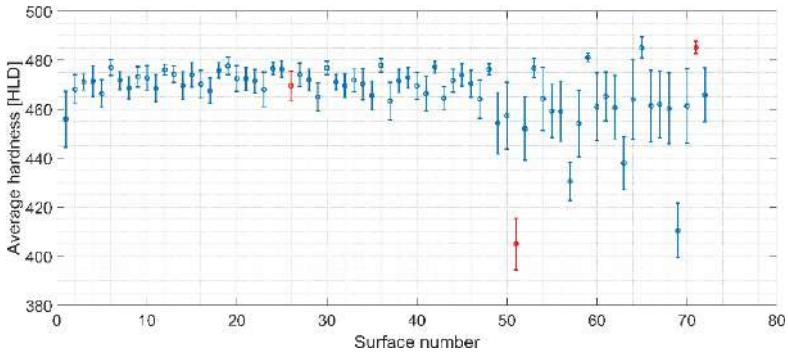


Figure 11 Selected surfaces for the calibration tests (see online version for colours)

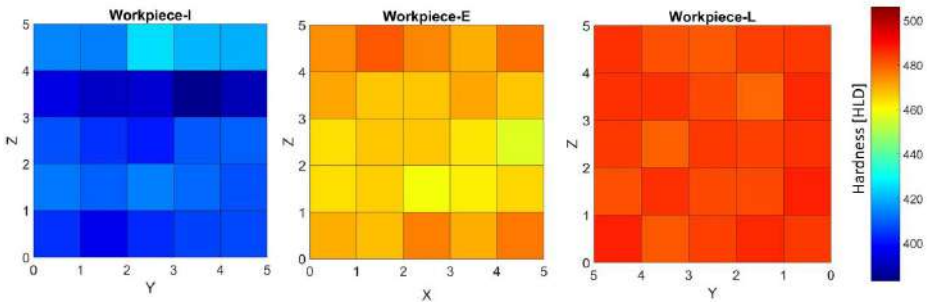
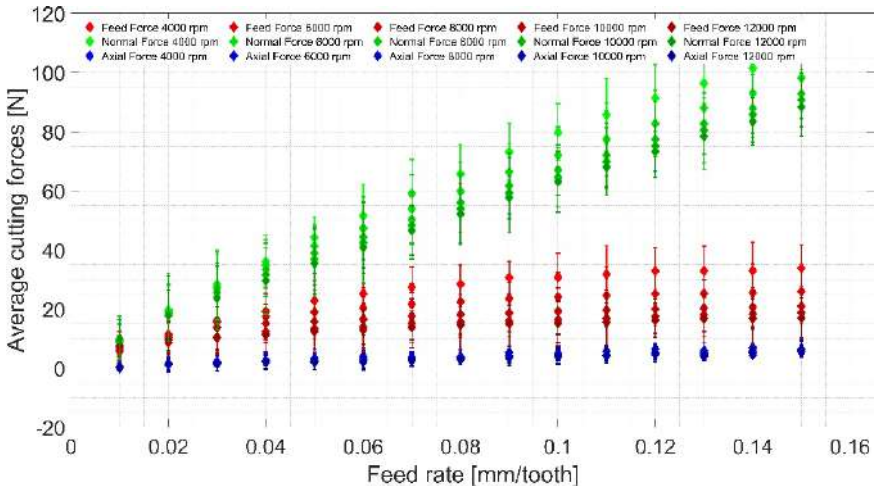


Figure 12 shows the average cutting forces measured for the surface 2 from the workpiece E, with the median hardness of 469 HLD. For the sake of brevity, the figures for the surfaces 1 with the minimum (405 HLD) and 2 with the maximum hardness (485 HLD) are not shown.

Figure 12 Average cutting forces for surface 2 with average hardness of 469 HLD (see online version for colours)



The resulting feed rate-dependent average cutting force coefficients for the surface 2 with the median hardness (460 HLD) are given in Figure 13. Again, the figures for the maximum (485 HLD) and minimum (405 HLD) hardness surfaces (surfaces 1 and 3) are not presented for the sake of brevity. For the calculation of the cutting coefficients, the mechanistic calibration method described by Altintas (2012) is used with the measured average cutting forces presented in Figure 12. In this method the average forces at each feed rate are measured and the cutting edge components ($\overline{F_{xe}}, \overline{F_{ye}}, \overline{F_{ze}}, \overline{F_{xc}}, \overline{F_{yc}}, \overline{F_{zc}}, \overline{F_{xe}}, \overline{F_{ye}}, \overline{F_{ze}}, \overline{F_{xc}}, \overline{F_{yc}}, \overline{F_{zc}}$) are estimated by a linear regression of the data. The cutting force coefficients are then evaluated as follows:

$$\begin{aligned}
 K_{tc} &= \frac{\overline{4F_{yc}}}{Na_p}, & K_{te} &= \frac{\overline{\pi F_{ye}}}{Na_p}, \\
 K_{rc} &= \frac{\overline{-4F_{xc}}}{Na_p}, & K_{re} &= \frac{\overline{-\pi F_{xe}}}{Na_p}, \\
 K_{ac} &= \frac{\overline{\pi F_{zc}}}{Na_p}, & K_{ae} &= \frac{\overline{2F_{zc}}}{Na_p}.
 \end{aligned}
 \tag{11}$$

For each feed rate on Figure 13, first the selected average cutting forces presented in Figure 12 are used for linear regression. For example, for the first data point in Figure 13 ($f_z = 0.15$ mm/tooth), the average cutting forces measured for $f_z = 0.10$ mm/tooth and $f_z = 0.20$ mm/tooth shown on Figure 12 are used for linear regression. The slopes of these linear fits (one for feed and one for normal direction) are used to calculate the average cutting force coefficients for $f_z = 0.15$ mm/tooth. For the next feed rate $f_z = 0.25$ mm/tooth, the linear regression is applied to average cutting forces data between $f_z = 0.10$ mm/tooth and $f_z = 0.30$ mm/tooth. For $f_z = 0.35$ mm/tooth from $f_z = 0.10$ mm/tooth to $f_z = 0.40$ mm/tooth and so on.

Figure 13 Average cutting force coefficients measured on the surface 2 with average hardness of 469 HLD (see online version for colours)

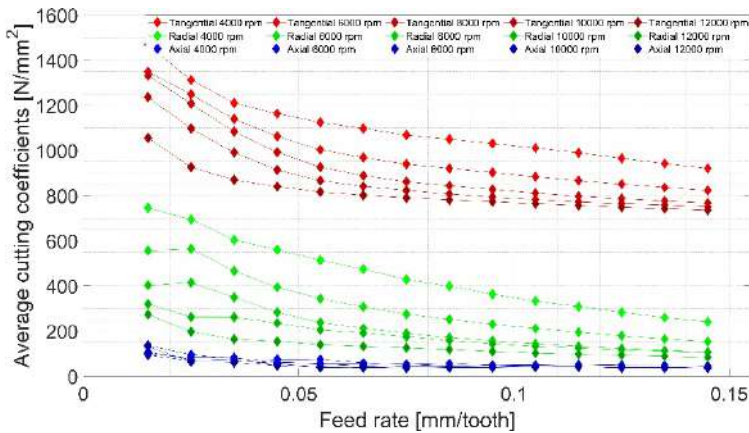
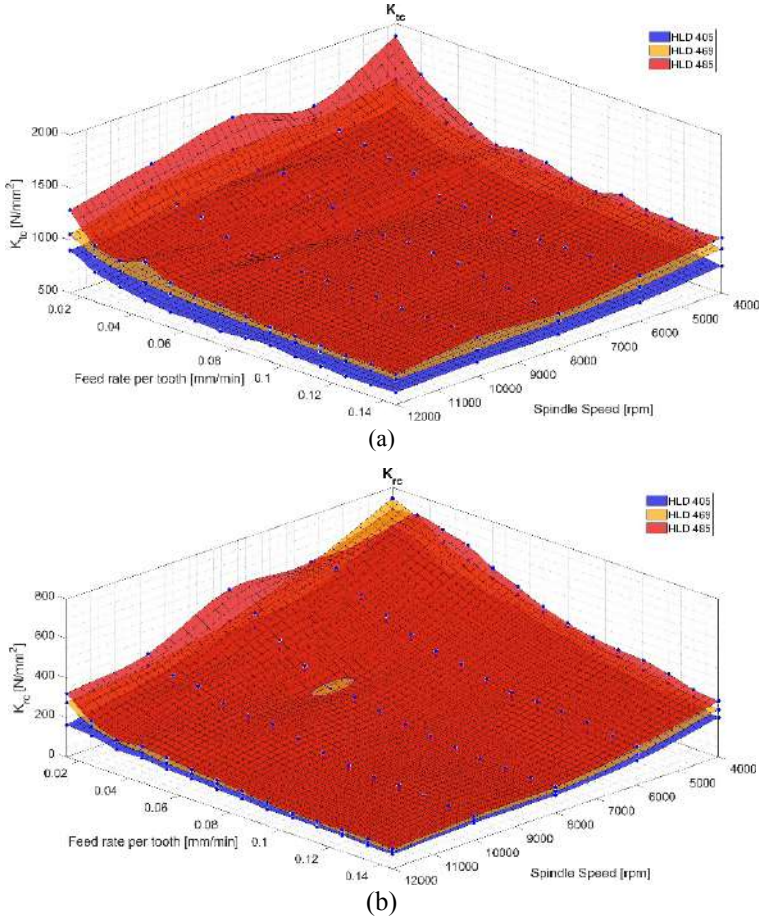


Figure 14 (a) 3D surface representation of tangential cutting coefficient and (b) 3D surface representation of radial cutting coefficient (see online version for colours)



The variation of tangential and radial cutting coefficients with respect to spindle speed and feed rate for different hardness values are presented in Figure 14(a) and (b) using cubic spline interpolation to generate the surfaces for illustration purposes. Figure 14(a) and (b) indicate that the behaviour of the cutting coefficients with respect to spindle speed and feed rate is nonlinear, whereas, with respect to hardness, it is linear. Campatelli and Scippa (2012) also studied the variation of the cutting coefficients with respect to spindle speed and feed rate in milling Al-6082 alloy. They assumed a nonlinear relation between the coefficients and the feed rate, but they preferred a linear correlation between the cutting coefficients and the spindle speed to generate a surface to predict the tangential cutting coefficients. However, the most significant error between the predicted coefficients and the experiments occurred at low cutting speeds. The authors commented that a more complex relationship than a linear correlation between the cutting speed and tangential cutting coefficient should be investigated.

Therefore, in this study, it is assumed that the relations between cutting coefficients-spindle speed and the cutting coefficients-feed rate are both nonlinear and the cutting coefficients- hardness is linear. Then, the function of the tangential cutting coefficient

with respect to spindle speed n [rpm], feed rate f_z [mm/min], and Leeb hardness H_{HLD} [HLD] takes the following form:

$$K_{ic} = C_1 n^{-C_2} + C_3 f_z^{-C_4} + C_5 H_{HLD} + C_6. \quad (12)$$

Similarly, the relation for the radial cutting coefficient would be as follows:

$$K_{rc} = C_7 n^{-C_8} + C_9 f_x^{-C_{10}} + C_{11} H_{HLD} + C_{12}. \quad (13)$$

The constants $C_1 \dots C_{12}$ are given in Table 3. They are calculated using nonlinear least-squares regression.

Table 3 Values of the constants $C_1 \dots C_{12}$ in equations (12) and (13)

| C_1 | C_2 | C_3 | C_4 | C_5 | C_6 |
|--------|---------|--------|----------|----------|----------|
| -560 | -0.132 | -58292 | -0.0036 | 3.283 | 58979 |
| C_7 | C_8 | C_9 | C_{10} | C_{11} | C_{12} |
| -68587 | -0.0037 | -1200 | -0.251 | 0.864 | 71398 |

Once the hardness-dependent cutting coefficients are determined, local stability conditions can be predicted. In order to validate this approach, Workpiece L was used since it has an asymmetrical “U-shaped” hardness profile similar to the workpiece shown in Section 2, the workpiece being harder on the sides and softer in the center. Figure 15 gives an overview of the validation cuts. The cutting conditions for these cuts are given in Table 4.

Table 4 Process parameters of the validation cuts

| <i>Parameter</i> | <i>Value</i> |
|------------------|----------------|
| Spindle speed | 8000–17000 rpm |
| Feed rate | 0.05 mm/tooth |
| a_p | 0.25–0.6 mm |
| a_e | 12 mm |
| Number of flutes | 4 |
| Stick-out length | 55 mm |
| Feed direction | X^+ , Y^+ |

Three sample cuts for each stability state from Figure 15 are shown in Figures 16–18 using time-frequency power spectrum plots. The colour of the signal indicates its power at any given time and frequency. The power of the signal is calculated by taking the square of the signal and normalising it for the time window, therefore has the unit of [dB].

In Figure 16, it is seen that the dominant frequency during the cut lies on the dashed white lines, which indicate the tooth passing frequency and its harmonics, indicating there is no regenerative vibration.

In Figure 17, the dominant frequency during the cut was 2080 Hz which is not a harmonic of the tooth passing frequency indicating the existence of chatter.

Figure 15 Overview of the validation cuts with varying stability at the border (see online version for colours)

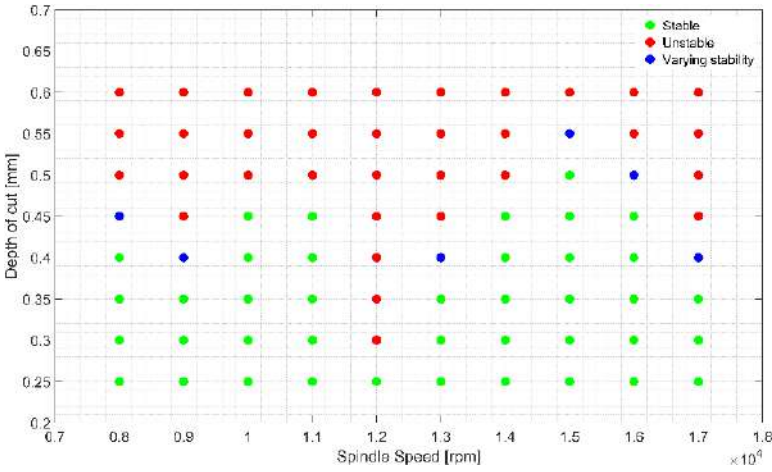


Figure 16 A sample time-frequency plot for a stable cut. The spindle speed is 10,000 rpm, feed rate is 0.05 mm/tooth and the depth of cut is 0.4 mm (see online version for colours)

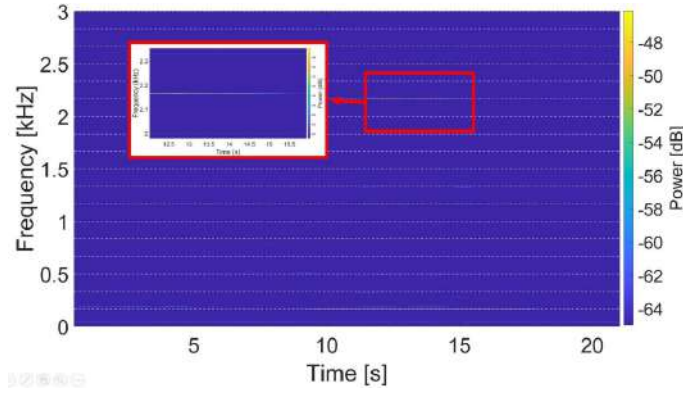


Figure 17 A sample time-frequency plot for an unstable cut. The spindle speed is 12,000 rpm, feed rate is 0.05 mm/tooth and the depth of cut is 0.5 mm (see online version for colours)

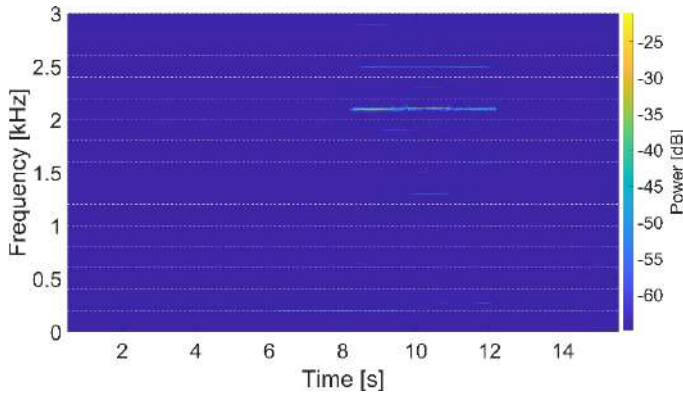
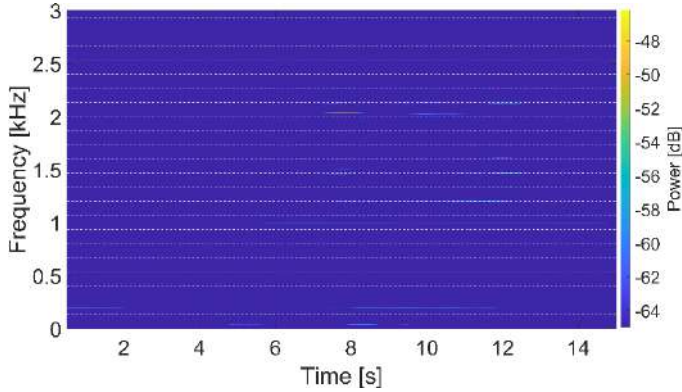


Figure 18 A sample time-frequency plot for a cut with varying stability. The spindle speed is 8000 rpm, feed rate is 0.05 mm/tooth and the depth of cut is 0.45 mm (see online version for colours)



In Figure 18, it is seen that chatter at 2078 Hz started with the beginning of the cut at the seventh second, stopped towards the middle of the cut and restarted towards the end of the cut, similar to the case described in Section 2.

In order to predict the occurrence of this varying stability, local hardness dependent average cutting force coefficients were calculated with $n = 8000$ rpm and $f_z = 0.05$ mm/tooth into the hardness dependant cutting coefficient relations with Equation 14:

$$\begin{aligned}
 K_{fc} [\text{N/mm}^2] &= 3.283HLD - 120.3, \\
 K_{rc} [\text{N/mm}^2] &= 0.864HLD + 253.8
 \end{aligned}
 \tag{14}$$

Figure 19 shows the corresponding hardness-dependent stability lobe diagram. The data tips indicate the limit depth of cut for the hardness of 400 HLD and 500 HLD.

Figure 19 Hardness dependent SLD (see online version for colours)

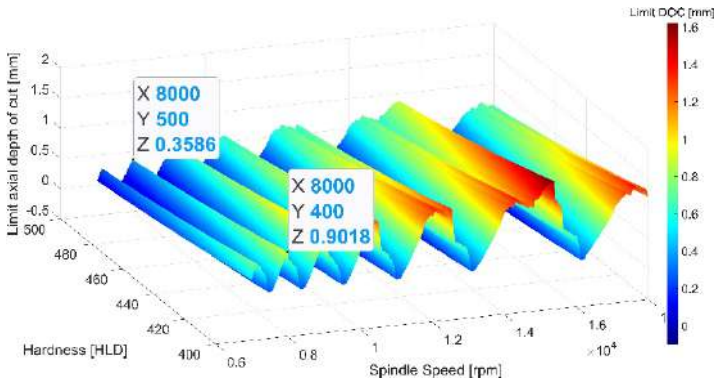
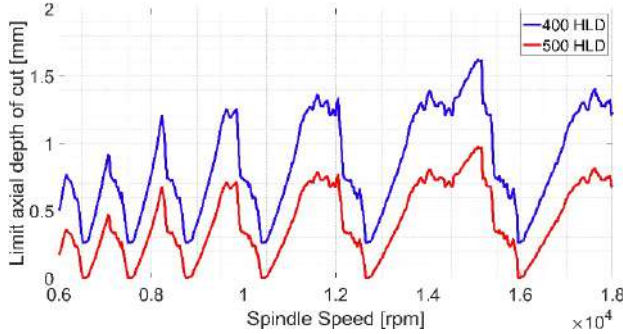


Figure 20 compares the SLDs with the coefficients corresponding to the highest (500 HLD) and lowest (400 HLD) hardness values. From Figure 20 it can be seen that the change in hardness shifts the stability limits in the vertical direction but does not affect

the general shape of the limits, since the hardness has a linear effect on the stability lobe through the linear increase of the cutting coefficients.

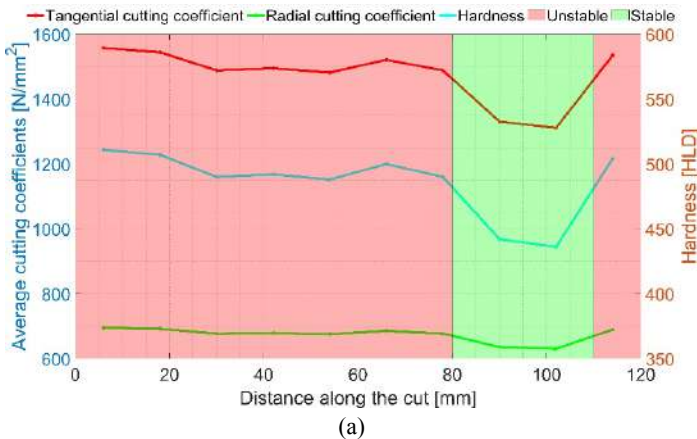
Figure 20 Comparison of the SLDs for 400 HLD and 500 HLD (see online version for colours)



The described method was validated using the following experiments, which were conducted at $n = 8000$ rpm and $f_z = 0.05$ mm/tooth per tooth, at which the stability is changing around 483 HLD, as shown in Figure 19. In the following figures, results from these experiments are shown. For each case, first, the hardness variation, corresponding local cutting coefficient variation, and the predicted stability along the cut are shown. Then in the second figure, the measured sound spectrum during the cut is shown along with the stable and unstable regions during the cut.

Figure 21 shows how the hardness was dropping towards the end of cut around 80 mm before it sharply increased again around 110 mm, which indicates a stable zone in between. This was indeed the case, as shown in Figure 21 as the chatter frequency of 2030 Hz died out towards the 16 s mark and reoccurred around 16.6 s. Also, in the first unstable region, the local hardness was at its maximum at the beginning of the cut. Similarly, the chatter violence indicated by signal loudness was higher in this region, as indicated by a brighter colour, compared to the rest of the unstable zone.

Figure 21 (a) Hardness variation, corresponding average cutting coefficients, and predicted stable and unstable zones for validation cut 1 and (b) sound spectrum of validation cut 1 with detected stable and unstable zones. Spindle speed is 8000 rpm and the feed rate is 0.05 mm/tooth (see online version for colours)



(a)

Figure 21 (a) Hardness variation, corresponding average cutting coefficients, and predicted stable and unstable zones for validation cut 1 and (b) sound spectrum of validation cut 1 with detected stable and unstable zones. Spindle speed is 8000 rpm and the feed rate is 0.05 mm/tooth (see online version for colours) (continued)

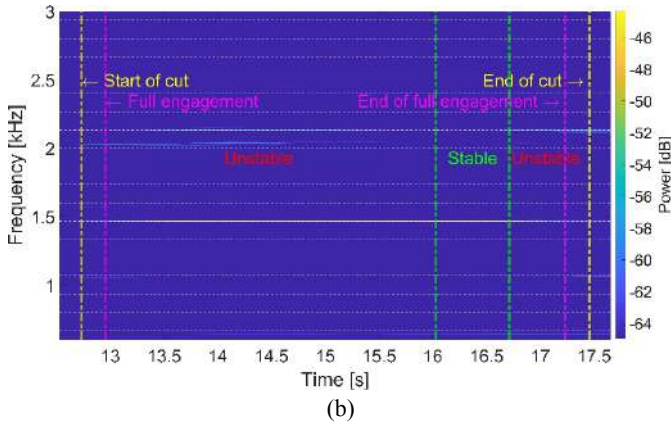
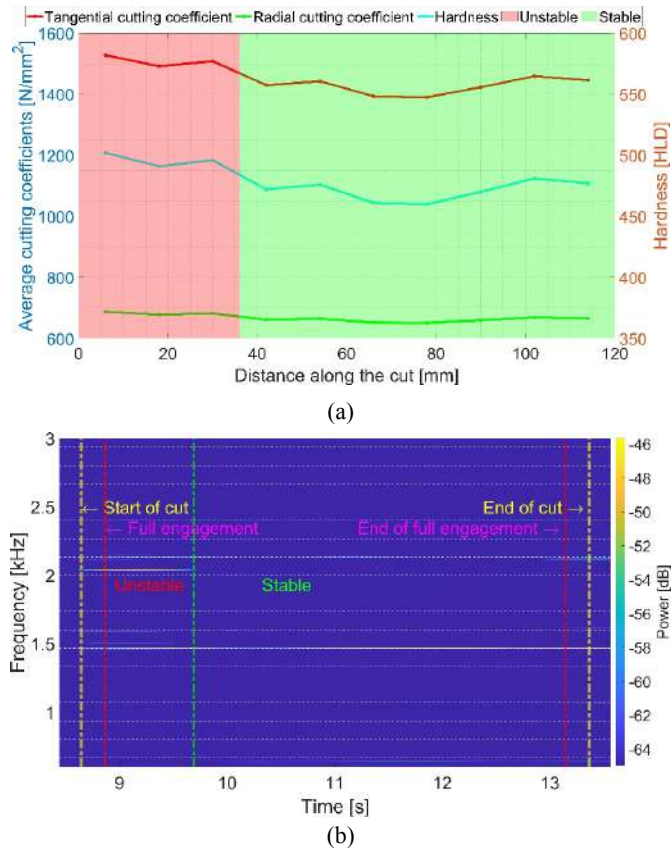


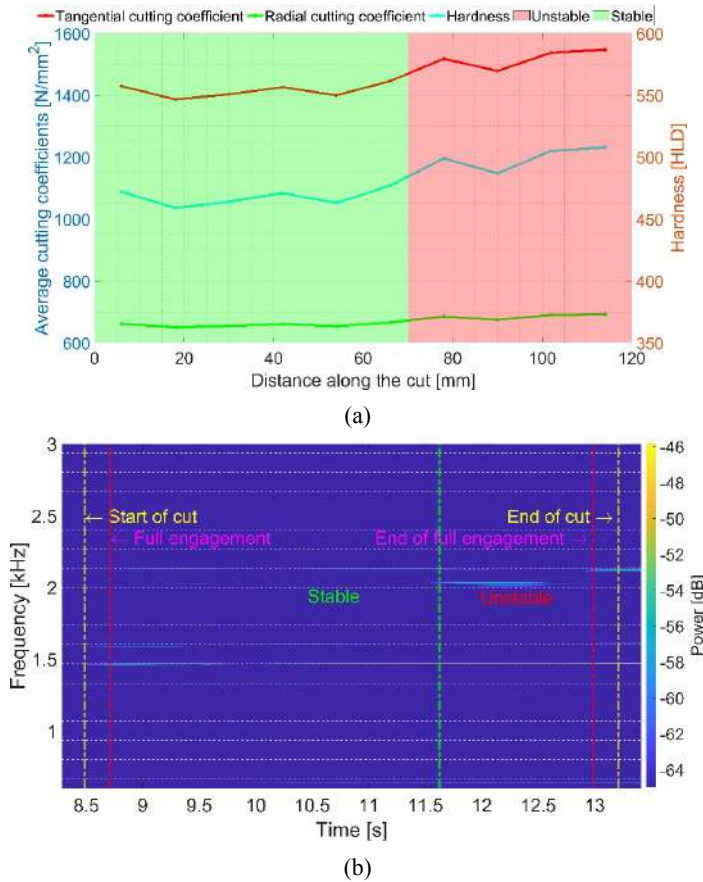
Figure 22 (a) Hardness variation, corresponding average cutting coefficients, and predicted stable and unstable zones for validation cut 2 and (b) sound spectrum of validation cut 2 with detected stable and unstable zones. Spindle speed is 8000 rpm and the feed rate is 0.05 mm/tooth (see online version for colours)



In Case 2, the hardness values dropped below the critical value and remained there, as shown in Figure 22. In such a case, once the chatter vibrations are damped, they do not restart as in the previous cases. In this cut, the drop below the critical hardness occurred around 35 mm, which was approximately 1 second after the cutter entered the workpiece.

Case 3 shows a case where the hardness values increased above the critical value around the middle of the workpiece and remained high from that point on, as shown in Figure 23. In such cases, chatter vibrations tend to start at the middle of the cut and continue until the end of full cutter engagement.

Figure 23 (a) Hardness variation, corresponding average cutting coefficients, and predicted stable and unstable zones for validation cut 3 and (b) sound spectrum of validation cut 3 with detected stable and unstable zones. Spindle speed is 8000 rpm and the feed rate is 0.05 mm/tooth (see online version for colours)



6 Conclusion

In this paper, the effect of workpiece material inhomogeneity on chatter stability is investigated. The workpiece and the cutting conditions used in this study were selected

according to the real-life problems in industry. The workpieces, which were ordered from a commercial material supplier, showed inhomogeneous behaviour due to effects remaining from primary manufacturing. The inhomogeneity of the workpieces was not known a priori to the milling operations, thus the experimental stability limits deviated from the theoretical limits. In order to identify the root cause of the deviations, first the surface hardness of the workpieces were measured using rebound hardness tests. Then, experimentally determined cutting coefficients were correlated with the measured hardness. It is shown that the local hardness of the workpiece material affects the local cutting coefficients and thus, the local chatter stability. Once the relation between the cutting coefficients and the hardness is established, this relation can be used to predict the stability limits for workpiece with changing hardness. Especially for batch production, where the individual workpieces show varying inhomogeneity, the cutting coefficients can be calibrated for a single workpiece and for the rest of the batch, the hardness can be measured rather than the cutting forces. The coefficients can then be calibrated by only correlating the hardness measurements without the need for a cutting force dynamometer.

This study focuses on the measured hardness values to determine the material inhomogeneity. For future studies, the effect of factors such as plastic deformation and grain size on cutting coefficients and chatter stability can also be investigated. In addition, this study can be combined with real time process monitoring applications and extended to automatic detection of workpiece inhomogeneity. By monitoring the cutting process in real-time, the change in local workpiece material properties can be identified and the cutting coefficients can be updated. Using such an approach the occurrence of chatter can be avoided to ensure stable milling operations and the process parameters can be updated to achieve higher productivity.

References

- Aggarwal, S. (2012) *Part Programming to Realize Chatter Free and Efficient High Speed Milling*, EPFL, PhD Thesis.
- Aggarwal, S., Nevsic, N. and Xirouchakis, P. (2012) 'Part programming to realize chatter free and efficient high speed milling', *The International Journal of Advanced Manufacturing Technology*, Vol. 65, pp.81–95.
- Altintas, Y. (1992) 'Prediction of cutting forces and tool breakage in milling from feed drive current measurements', *Journal of Engineering for Industry*, Vol. 114, No. 4, pp.386–392.
- Altintas, Y. (2012) *Manufacturing Automation: Metal Cutting Mechanics, Machine Tool Vibrations, and CNC Design*, Cambridge University Press, Cambridge, UK.
- Altintas, Y., Kersting, P., Biermann, D., Budak, E., Denkena, B. and Lazoglu, I. (2014) 'Virtual process systems for part machining operations', *CIRP Annals*, Vol. 63, pp.585–605.
- Arrazola, P.J., Ozel, T., Umbrello, D., Davies, M. and Jawahir, I.S. (2013) 'Recent advances in modelling of metal machining processes', *CIRP Annals*, Vol. 62, pp.695–718.
- Berezvai, S., Molnar, T.G., Bachrathy, D. and Stepan, G. (2018) 'Experimental investigation of the shear angle variation during orthogonal cutting', *Materials Today: Proceedings*, Vol. 5, No. 13, pp.26495–26500.
- Budak, E., Altintas, Y. and Armarego, Eja (1996) 'Prediction of milling force coefficients from orthogonal cutting data', *Journal of Manufacturing Science and Engineering*, Vol. 118, pp.216–224.
- Budynas, R.G.J., Nisbett, K. and Shigley, J.E. (2011) *Shigley's Mechanical Engineering Design*, 9th ed., McGraw-Hill, New York.

- Campatelli, G. and Scippa, A. (2012) 'Prediction of milling cutting force coefficients for aluminum 6082-T4', *Procedia CIRP*, Vol. 1, pp.563–568.
- Campocasso, S., Poulachon, G., Bissey-Breton, S., Costes, J.P. and Outeiro, J.C. (2017) 'Towards cutting force evaluation without cutting tests', *CIRP Annals*, Vol. 66, pp.77–80.
- Costa, M.I., Rodrigues, D.M. and Leitaó, C. (2015) 'Analysis of AA 6082-T6 welds strength mismatch: stress vs. hardness relationships', *The International Journal of Advanced Manufacturing Technology*, Vol. 79, Nos. 5–8, pp.719–727.
- Denkena, B., Kruger, M. and Schmidt, J. (2014) 'Condition-based tool management for small batch production', *The International Journal of Advanced Manufacturing Technology*, Vol. 74, pp.471–480.
- Denkena, B., Vehmeyer, J., Niederwestberg, D. and Maass, P. (2014) 'Identification of the specific cutting force for geometrically defined cutting edges and varying cutting conditions', *International Journal of Machine Tools and Manufacture*, Vol. 82, pp.42–49.
- Gomez, M., No, T., Smith, S. and Schmitz, T. (2020) 'Cutting force and stability prediction for inserted cutters', *Procedia Manufacturing*, Vol. 48, pp.443–451.
- Grossi, N., Sallese, L., Scippa, A. and Campatelli, G. (2014) 'Chatter stability prediction in milling using speed-varying cutting force coefficients', *Procedia CIRP*, Vol. 14, pp.170–175.
- Grossi, N., Sallese, L., Scippa, A. and Campatelli, G. (2014) 'Speed-varying cutting force coefficient identification in milling', *Precision Engineering*, Vol. 42, pp.321–334.
- Honeycutt, A. and Schmitz, T. (2019) 'Milling bifurcations for strongly asymmetric, symmetric, and weakly asymmetric system dynamics', *Precision Engineering*, Vol. 55, pp.1–13.
- Layegh, S.E.K. and Lazoglu, I. (2012) 'A new identification method of specific cutting coefficients for ball end milling', *Procedia CIRP*, Vol. 14, pp.182–187.
- Mrówka-Nowotnik, G., Sieniawski, J. and Nowotnik, A. (2009) 'Effect of heat treatment on tensile and fracture toughness properties of 6082 alloy', *Journal of Achievements in Materials and Manufacturing Engineering*, Vol. 32, No. 2, pp.162–170.
- No, T., Gomez, M., Smith, S. and Schmitz, T. (2020) 'Cutting force and stability for inserted cutters using structured light metrology', *Procedia CIRP*, Vol. 93, pp.1538–(1545).
- Pérez-Ruiz, D.J., López de Lacalle, L.N., Urbikain, G., Pereira, O., Martínez, S. and Bris, J. (2021) 'On the relationship between cutting forces and anisotropy features in the milling of LPBF Inconel 718 for near net shape parts', *International Journal of Machine Tools and Manufacture*, Vol. 170, p.103801.
- Standard, Iso (2016) 'Metallic materials – Leeb hardness test – 1: test method', *International Organization for Standardization*, 16859-1.
- Stepan, G., Dombovari, Z. and Munoa, J. (2011) 'Identification of cutting force characteristics based on chatter experiments', *CIRP Annals*, Vol. 60, pp.113–116.
- Urbikain, G.P. and Olvera, D.T. (2020) 'Model-based phase shift optimization of serrated end mills: Minimizing forces and surface location error', *Mechanical Systems and Signal Processing*, Vol. 144, p.106860.